Supporting Information:

Synergizing Plasmonic Au Nanocages with 2D MoS$_2$ Nanosheets for Significant Enhancement in Photocatalytic Hydrogen Evolution

Rui Peng[a,†], Xiaohan Ma[a,b,†], Zachary D. Hood[a,c], Abdelaziz Boulesbaa[d], Alex Puretzky[a], Jianhua Tong[b], and Zili Wu*[a]

[a] Center for Nanophase Materials Sciences, Oak Ridge National Laboratory, Oak Ridge, Tennessee 37831, United States

[b] Department of Materials Science and Engineering, Clemson University, Clemson, South Carolina 29634, United States

[c] Applied Materials Division, Argonne National Laboratory, 9700 S. Cass Avenue, Lemont, IL 60439, USA.

[d] Department of Chemistry & Biochemistry, California State University Northridge, Northridge, California 91330, United States

[†] Contributed equally to this work

*Address correspondence to: Zili Wu (wuz1@ornl.gov)
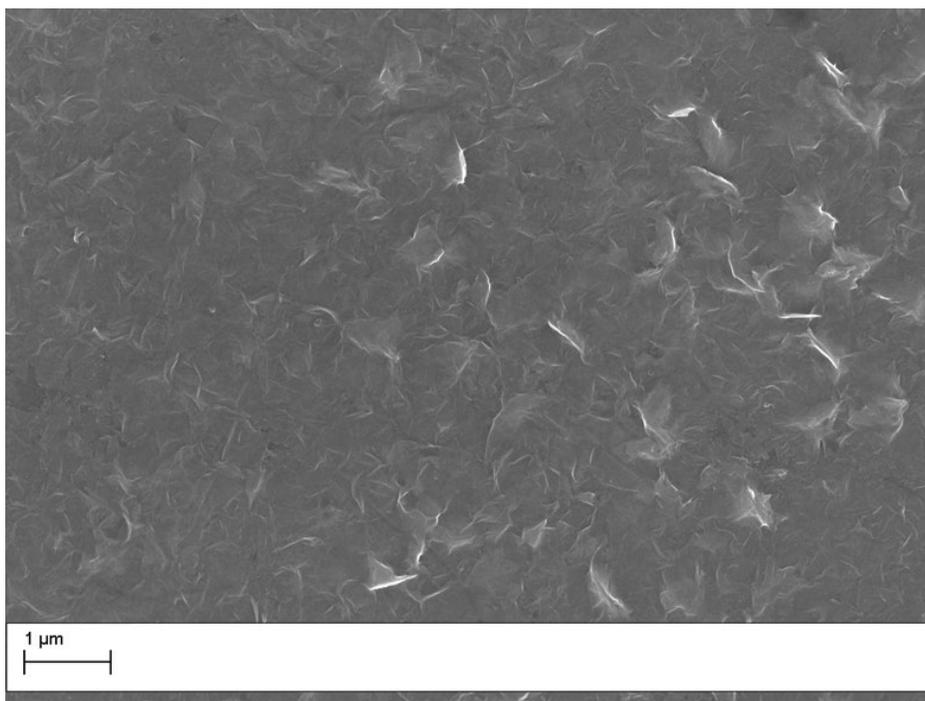
Figure S1. SEM image of exfoliated MoS$_2$ sample.
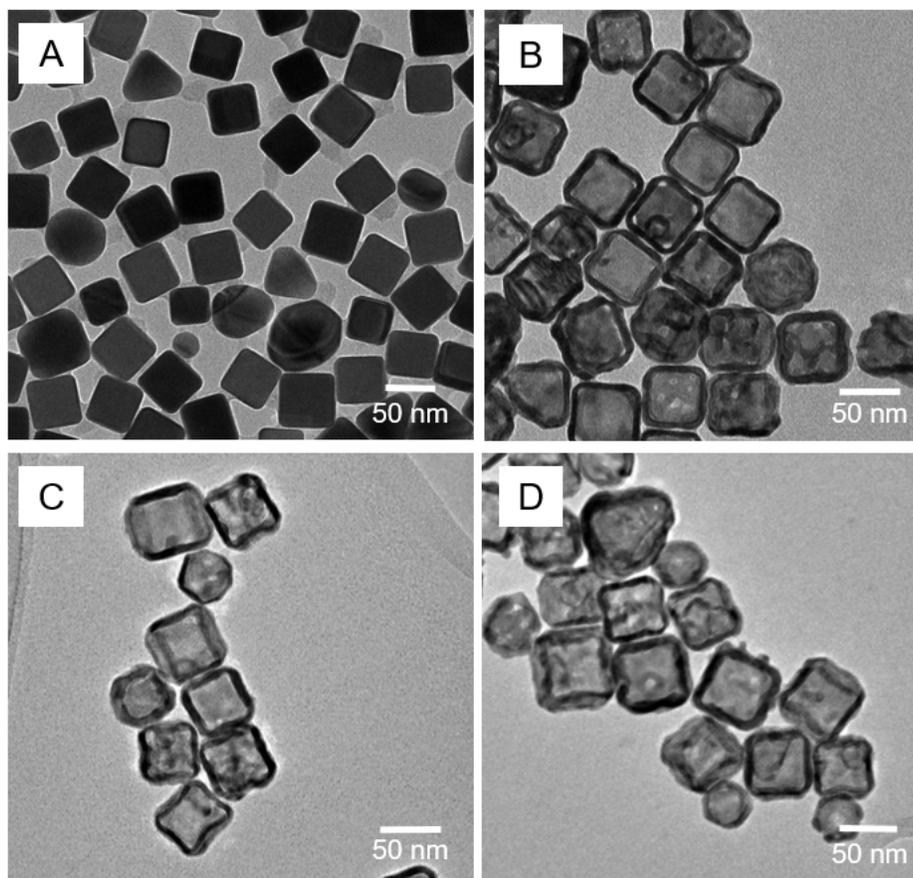
Figure S2. Representative TEM images of A) Ag nanocubes and Au nanocages with an LSPR at B) 460 nm, C) 680 nm, and D) 750 nm.
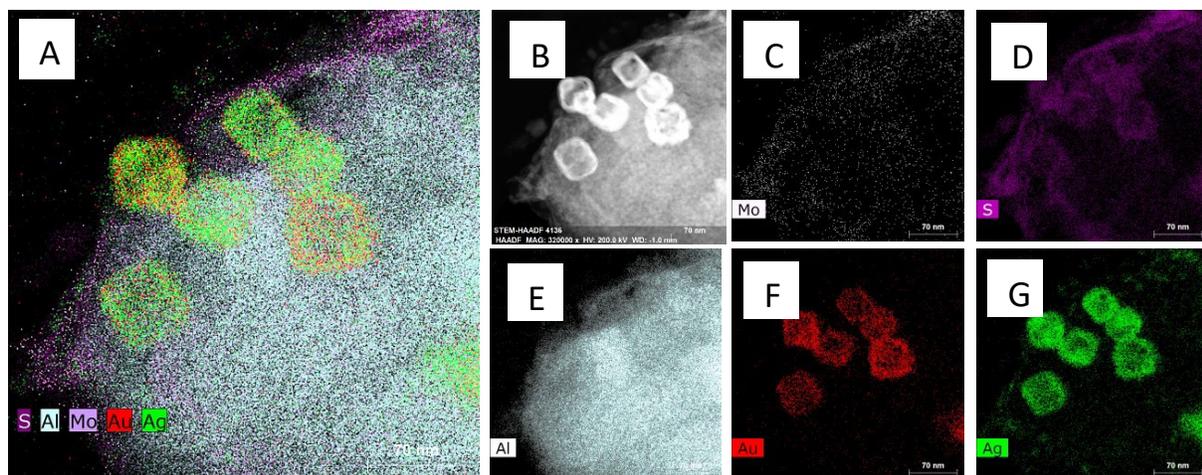
Figure S3. (A) STEM-EDS overall elemental map, (B) the corresponding STEM image and the individual mappings of (C) Mo (D) S (E) Al (F) Au and (G) Ag of AMA-680.
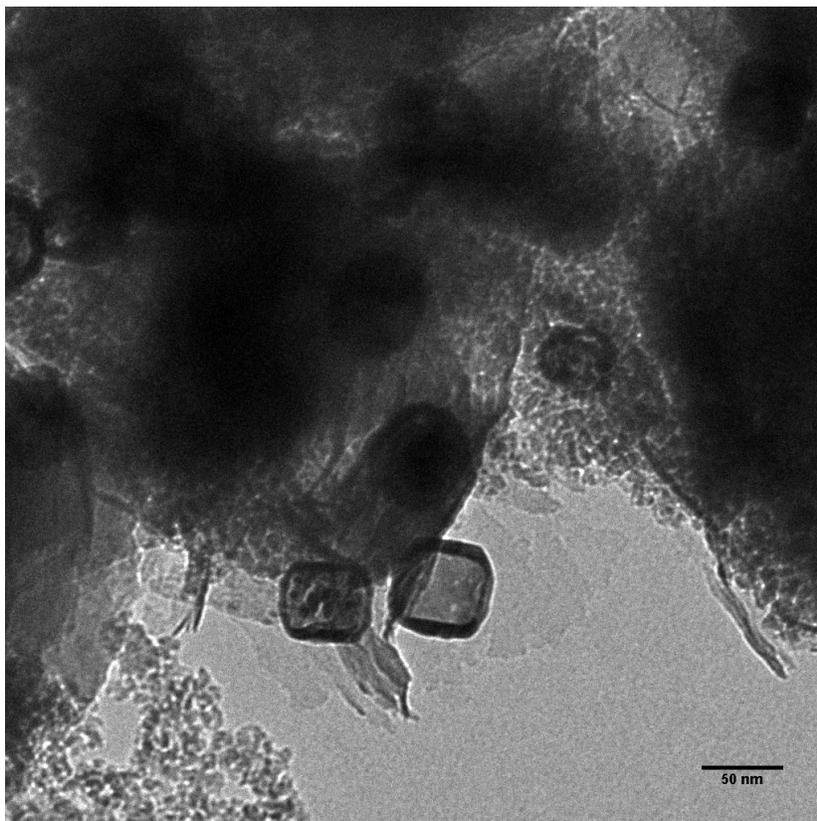
Figure S4. TEM image of the AMA-680-120 sample.
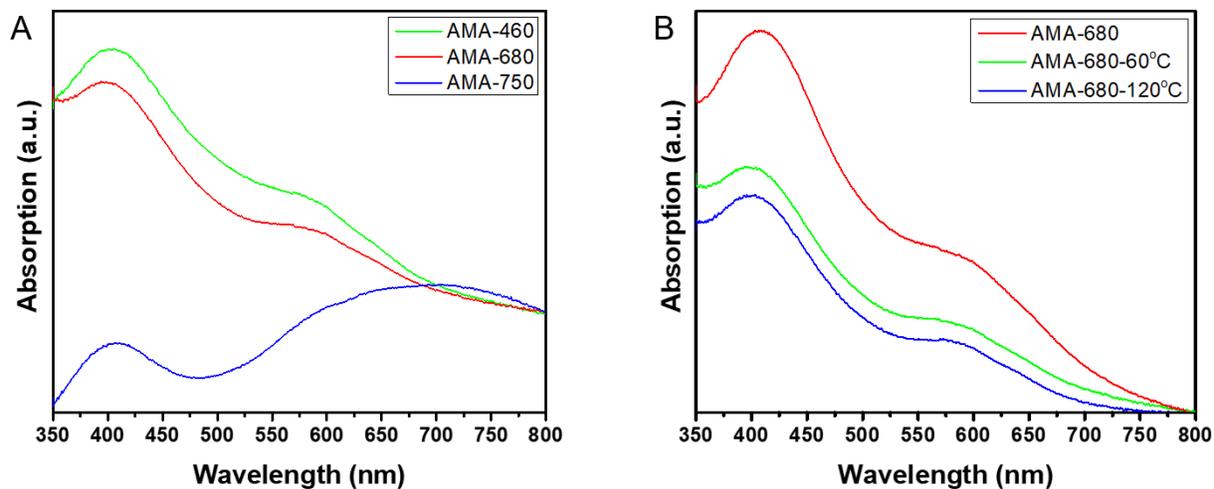
Figure S5. Diffuse reflectance spectra of A) AMA samples with various Au nanocages; B) AMA 680 samples treated at various temperatures.

Table S1. Relative fraction of 1T and 2H phases in different samples from XPS analysis.

Sample	Relative fraction	
	1T	2H
460 nm	0.59	0.41
680 nm	0.60	0.40
680 nm - 60 °C	0.53	0.47
680 nm - 120°C	0.45	0.55
750 nm	0.60	0.40

Table S2. Fitted results of three amplitudes (mOD) of the AMA samples monitored at 495 and 730 nm.

Amplitude	Au-680	MoS_2	AMA-460	AMA-680	AMA-750
A_1-495	8.3	-4.2	-2.6	-6.8	-1.9
A_1-730	-12.9	-1.9	-2.6	3.3	-2.1
A_2-495	-13.1	2.9	0.9	4.3	1.3
A_2-730	8.1	1.6	0.9	3.2	1.7
A_3-495	0.9	1.3	0.7	2.6	0.6
A_3-730	0.9	0.3	0.7	1.6	0.6

Discussion of the fitting results

By comparing the fitted time constants of the three AMA samples with bare MoS_2 nanosheets (shown in **Table 1** in the main text), it is found that they demonstrate three distinct behaviors.

For AMA-460, all the three time constants are seemingly not affected by LSPR, which suggests that the classic electron transfer from MoS_2 to Au nanocages is the dominant process in this system and the effect of LSPR is negligible, as shown in **Figure S6A**. This system is a classic photocatalyst system, where MoS_2 is the semiconductor and Au-460 works as cocatalyst.

For AMA-750, however, it is a much more complicated situation. Its decay dynamics is sensitive to the monitoring wavelength and starts to take the shape of bare MoS_2. This highly implies that the LSPR effect in this system becomes strong enough to nullify the contribution from the classic electron transfer. Specially, when monitoring at 730 nm, where LSPR is strong for Au-750, the t_1 of AMA-750 is slightly longer than MoS_2 while t_2 and t_3 are greatly shortened. Considering their above-mentioned indications, this clue suggests that the LSPR wins the competition, but just marginally. However, it completely changes the electron migration direction. Therefore, the whole system is then converted to a plasmonic photocatalyst system, as shown in **Figure S6C**. The strong LSPR effect under 730 nm intensively prohibited the classic electron transfer.

For AMA-680, its decay dynamics was also dependent on monitoring wavelength. However, unlike AMA-750, the decay behavior of AMA-680 was more analogous to Au nanocages, not MoS_2. This strongly suggested that this system was dominated by LSPR, as shown in **Figure S6B**. It is noteworthy that AMA-680 demonstrated the longest t_1 (t_1-730, 1.4 ns) of the three AMA samples. As t_1 is the indicator of LSPR effect, it means AMA-680 was influenced by LSPR most, which can account for its highest photocatalytic activity.
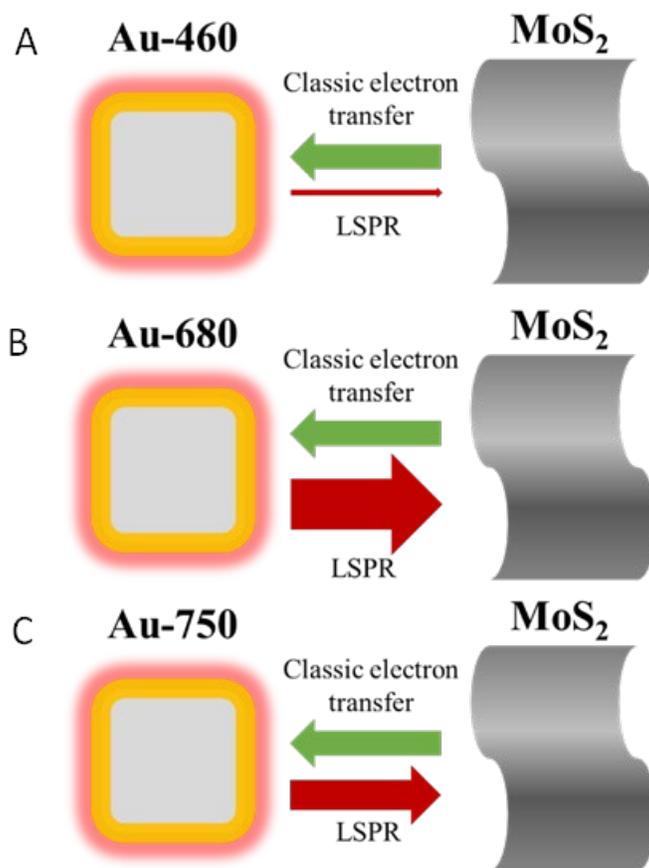
Figure S6 Schematic illustration of the electron transfer process in A) AMA-460, B) AMA-680 and C) AMA-750.